PLUME INDUCED AERODYNAMIC AND HEATING MODELS FOR THE LOW DENSITY SUPERSONIC DECELERATOR TEST VEHICLE

Brandon L. Mobley – MSFC EV33 Aerosciences, Huntsville, AL
Sheldon D. Smith – MSFC EV33 – Jacobs, Huntsville, AL
John W. Van Norman – LaRC – Analytical Mechanics Associates, Inc., Hampton, VA
Deepak Bose – ARC - Analytical Mechanics Associates, Inc., Mountain View, CA
Suman Muppidi – ARC - Analytical Mechanics Associates, Inc., Mountain View, CA
A. J. Mastropietro – JPL/Caltech – Thermal Systems, Pasadena, CA
Ian Clark – JPL/Caltech – LDSD Program Principle Investigator, Pasadena, CA

Presented By:

Brandon L. Mobley

Thermal & Fluids Analysis Workshop
TFAWS 2017
August 21-25, 2017
NASA Marshall Space Flight Center
Huntsville, AL

Agenda

- Background
- Analysis Objectives
- Approach
- Analyses
  - Spin Motor Plume Impingement Environments
  - Main SRM Plume Induced Environments
- Conclusions & Lessons Learned

Background

- LDSD Supersonic Flight Dynamics Tests (SFDT-1, 2)
  - Test supersonic deceleration technologies in Earth's upper stratosphere, SFDT-1: June 28, 2014, SFDT-2: June 8, 2015
  - Balloon launched test vehicle, accelerated using a solid rocket motor (SRM) to achieve freestream test conditions (simulate Mars entry)
  - SFDT-1 & 2 Deceleration Technologies
    - Supersonic Inflatable Aerodynamic Decelerator - Robotic class (SIAD-R)
    - Parachute Deployment Device (PDD) – Ballute – Parachute extraction
    - Supersonic Disk Sail (SFDT-1) , Ring Sail (SFDT-2) Parachutes
- Marshall Space Flight Center – EV33 Aerosciences - Roles
  - Program onset - provide plume induced heating predictions throughout powered flight (main solid)
  - Spin motor plume impingement (heating and impact pressures)
  - Plume induced aerodynamics predictions (post-SFDT-1/pre-SFDT-2)

Background

Full Scale Testing in Earth's Stratosphere– Simulating Mars Entry

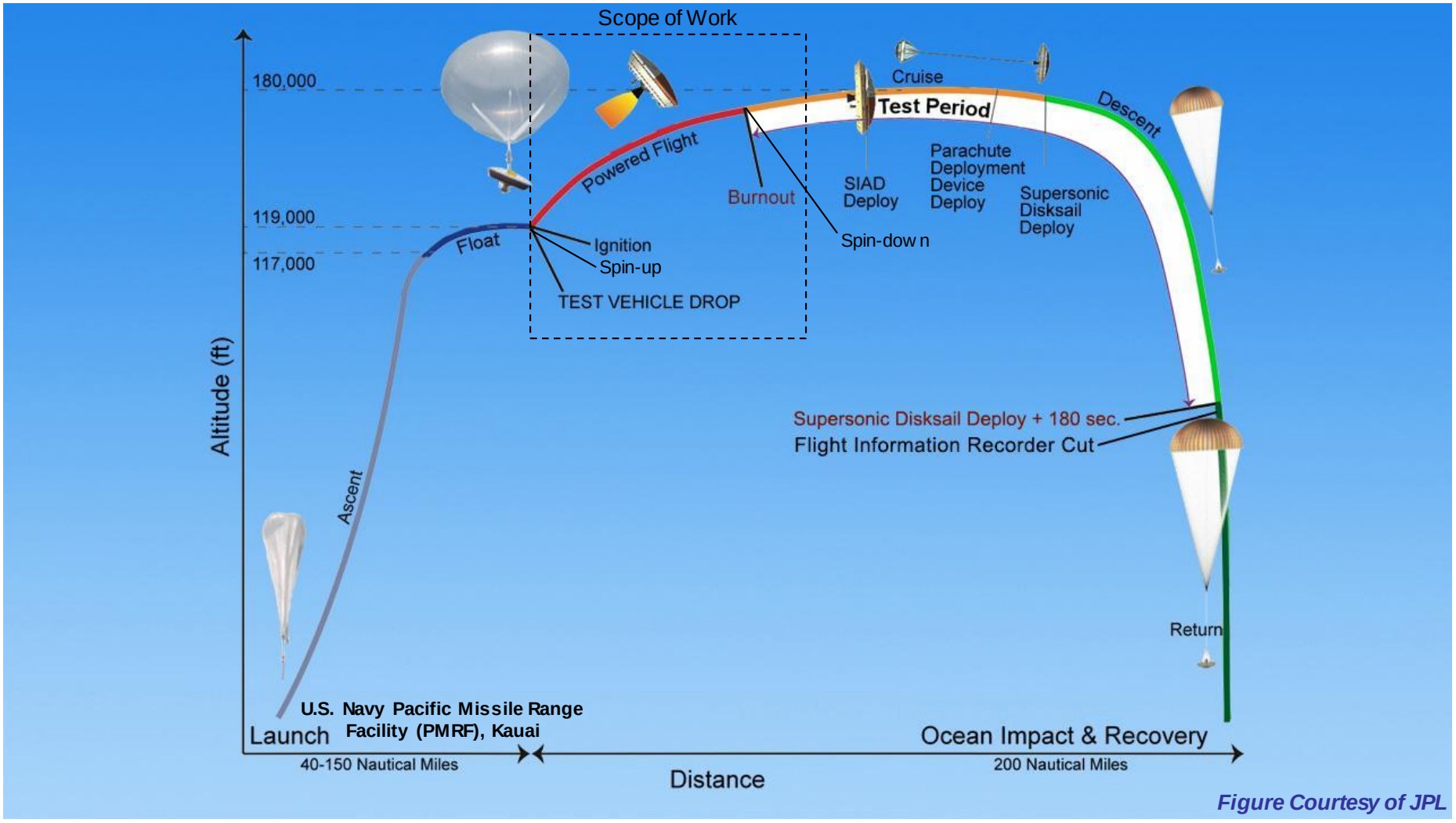

Figure Courtesy of JPL

Background

- LDSD Test Vehicle and Trajectories[1,2] (Best Equivalent)

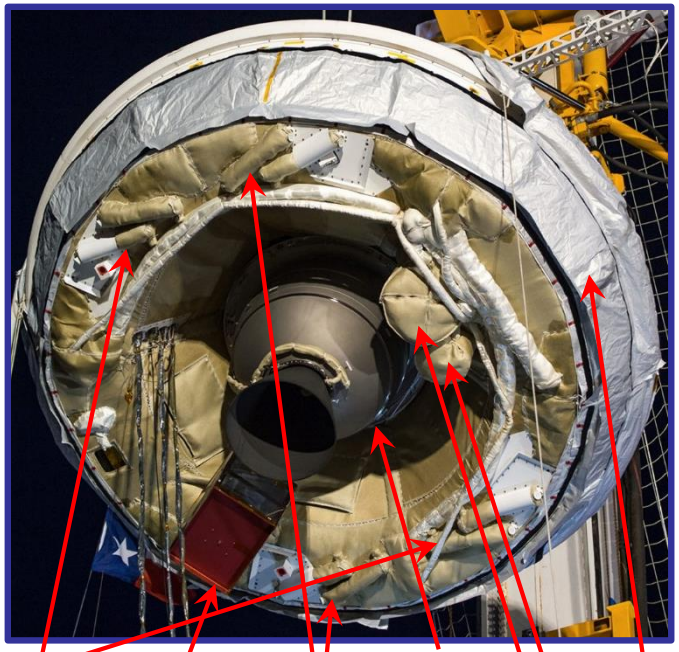

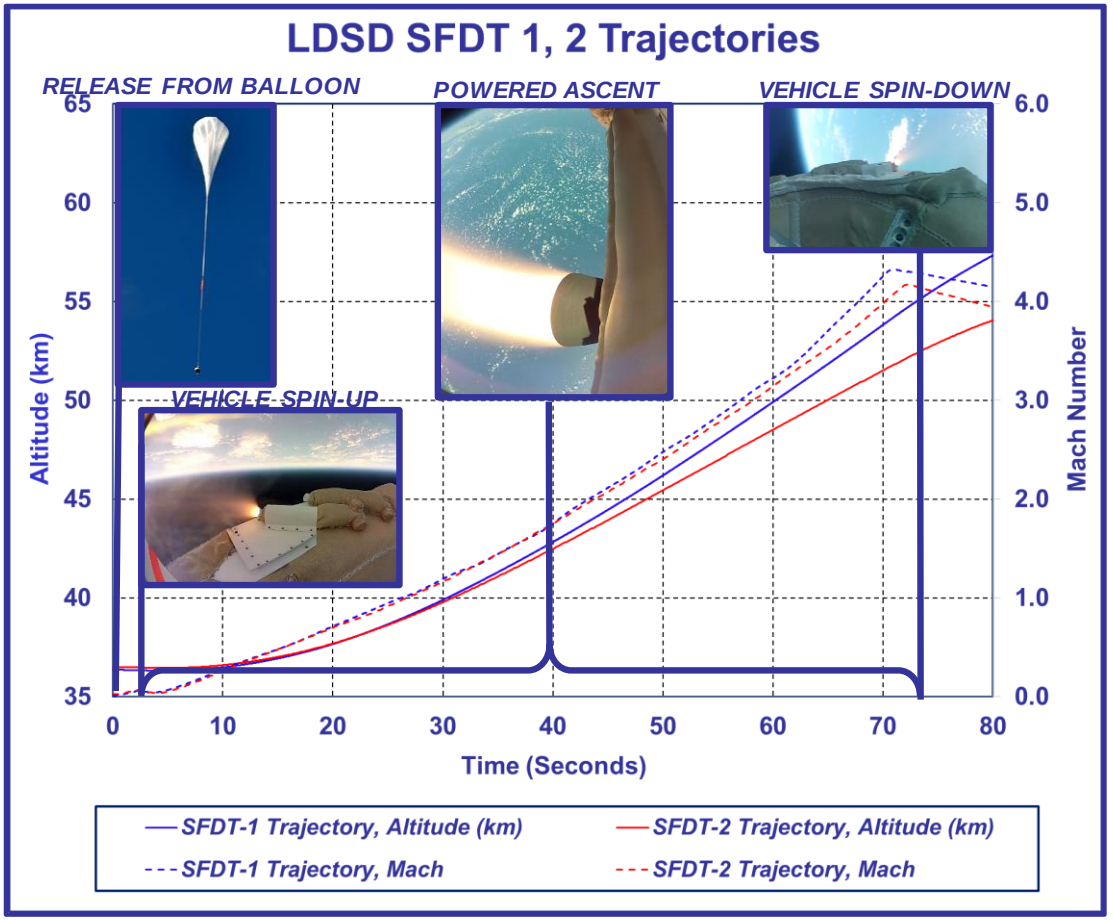

Background

Orbital-ATK Star-48B Long Nozzle Solid Rocket Motor[3]	
Expansion Ratio (A/A*)	54.8 (47.2 avg. nozzle erosion)
Throat Diameter	3.98 in / 10.11 cm
Exit Diameter	29.5 in / 74.93 cm
Nozzle Length	35.8 in / 90.93 cm
Chamber Pressure	Approximately 600 PSIA (@ t=0 sec)
Propellant (Approx. % Weight)	
71% Ammonium Perchlorate 11% Hydroxyl Terminated Polybutadiene (HTPB) 18% Aluminum	
Duration: Offloaded approx. 20% (400kg) to reduce burn time from 84 to 68 secs	

Nammo Talley, Inc. Solid Rocket Spin Motor	
Expansion Ratio (A/A*)	6.47
Throat Diameter	0.86 in / 2.2 cm
Exit Diameter	2.2 in / 5.59 cm
Nozzle Length	1.82 in / 4.63 cm
Chamber Pressure	Approximately 3057 PSIA
Propellant (Approx. % Weight)	
83% Ammonium Perchlorate 9% HTPB 5% Plasticizer	1.5% Aluminum 1.5% Fe_2O_3
Duration: 0.25 secs	

Analysis Objectives

- 2012–2013 LDSD Thermal Design Support
  - Star 48 Plume Induced Base Heating
    - Radiation heat flux from Al_2O_3 particles and plume gases
    - Convection from plume-air recirculation
  - Spin Motor Plume Impingement
    - Predict plume heating from convection and Al_2O_3 particle impingement
    - Plume induced forces & moments (spin performance)
    - Primary concerns, impingement heating on SIAD, parachute bridles and mast cameras and instrumentation
- 2014–2015 Plume Induced Aerodynamics Support
  - Predict aerodynamic coefficients (forces & moments) during subsonic and transonic powered flight
  - Investigate plume flow field modeling sensitivities to aerodynamics

Approach

- Simulate plumes throughout a flight trajectory at discrete points in time in a quasi-steady fashion
  - Two step approach, nozzle flows using engineering codes
  - Nozzle solutions used as boundary conditions to CFD domain
- Nozzle Flow Field
  - Model chamber and nozzle flow field chemistry using the NASA Glenn Chemical Equilibrium Combustion[4,5] (CEC) program
  - Model two-phase nozzle flow, core and boundary layer, using the Reacting and Multiphase Program[6] (RAMP2) & Boundary Layer Integral Matrix Procedure[7] (BLIMPJ) eng. codes (MOC codes)
- CFD (induced forces & convection) - Loci-CHEM[8-14] 3.3 p4
- Spin Motor Plume Particle Heating – PLIMP[15] eng. code
- Plume Radiation (sep. series of plume solutions, Star 48)
  - RAMP2 & SPF3[16,17] – Gas and Al^2O^3 particle plume flow field
  - Reverse Monte Carlo[18-20] – Particle, gaseous band model code

Computational Grid

- CFD Grid Challenges
  - Approach – Generally, try to create one grid to accommodate many cases, opposed to #grids refined for each case
  - Variation of motor firing configurations (2, 4)
    - 1 spin-up and 1 spin-down grid to suit case
    - Tailored surface geometries per spin motor impingement, removed protuberances “behind motors”
  - Variable angles of attack
  - Subsonic / supersonic free stream conditions (shock refinement, aspiration refinement/convergence)

- Grid Generation
  - ANSA 14, Solid Mesh 5.9.9[21] – Surface Grids, Volume Setup
  - AFLR3[22] – Unstructured – Volume Grids

Approach

Summary of CFD Settings, RANS

Category	Model Setup		
Case Description	Spin-Up Motors	Spin-Down Motors	Star48B Motor
Number of Plumes Simulated	4 (all on) and 2 (staggered firing)		1
Angle-of-Attack, α, and Side-Slip, β, Angles	α = 163°, β = 0°	α = 0°, β = 0°	Various, per trajectory
Plume Chemistry	Frozen		
No. Species	2 - Equivalent air & plume gas		
Thermodynamic and Transport Properties			
Specific Heat, Cp	Thermally perfect gas, specie Cp varies with temperature, polynomial		
Viscosity and Conduction Models	Transport Fit (equivalent μ(T), k(T), per specie)		
Diffusion Model	Laminar-Schmidt		
Particle Model	None		Aluminum-Oxide
Type			Lagrangian (1 Case)
Number of Particle Bins & Sizes			5, 1.662 - 4.557μm
Turbulence Model	Menter's Shear Stress Transport, SST		
Compressibility Correction	Sarkar		
Urelax (m/s)	0.10		
Dt Max (sec)	Varied per case, generally 0.001 - 0.0001 sec		
Accuracy	2nd Order, steady-state solutions		
Surface Boundary Conditions	No slip, vehicle spin rate applied		
Wall Temperatures	255, 973, 1773 K		255 K
Vehicle Spin Rate	0	50 (RPM)	
Internal Nozzle Wall Thermal	Adiabatic Wall (Carbon Phenolic)		
Solver	Guass-Seidel		

Spin-Up Motor Surface Mesh (Final Iteration, 174M)

STAR 48 SFDT-2 & Spin Motor Case Conditions[12]

Trajectory Atmospheric Conditions					Chamber Conditions			Vehicle Attitude	Notes
Alt (km)	M_∞	q_∞ (Pa)	P_∞ (Pa)	T_∞ (K)	Po (psia)	P_{lip} (psia)	$\theta_{Press\ Exp\ Ratio}$	α_{Total} (deg)	
36.050	0.01	0.84	499.03	246.00	3057.00	70.10	968.52	163.0	SPIN MTR, PRE-SFDT-1
36.322	0.10	3.46	494.00	242.00	643.68	1.61	22.54	40.4	Post-SFDT-1, Star 48, ADB
36.390	0.20	13.71	489.69	241.88	643.68	1.61	22.74	30.0	Post-SFDT-1, Star 48, ADB
36.514	0.30	30.30	481.00	242.00	643.68	1.61	23.15	22.3	Post-SFDT-1, Star 48, ADB
36.993	0.50	78.75	450.00	244.00	606.29	1.57	24.01	17.7	Post-SFDT-1, Star 48, ADB
37.617	0.70	141.66	413.00	244.00	607.40	1.59	26.46	17.1	Post-SFDT-1, Star 48, ADB
38.449	0.90	208.66	368.00	246.00	607.40	1.59	29.70	14.7	Post-SFDT-1, Star 48, ADB
38.682	0.95	225.53	357.00	248.00	607.40	1.59	30.61	14.4	Post-SFDT-1, Star 48, ADB
39.469	1.10	271.04	320.00	253.00	616.23	1.68	36.17	12.7	Post-SFDT-1, Star 48, ADB
49.480	4.23	1171.60	93.10	266.96	3057.00	70.10	5191.44	0.0	SPIN MTR, PRE-SFDT-1

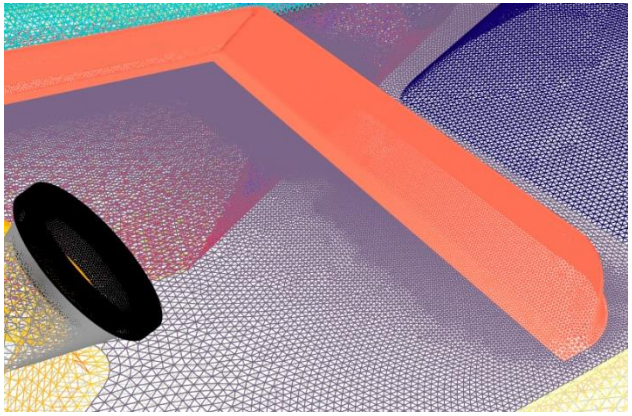

Spin Motor Analysis

INITIAL ANALYSIS

SPIN-UP – 120 Kft (36.6 km), P_∞= 0.72 PSIA (499 Pa) - ALL SPIN-UP MOTORS "ON"

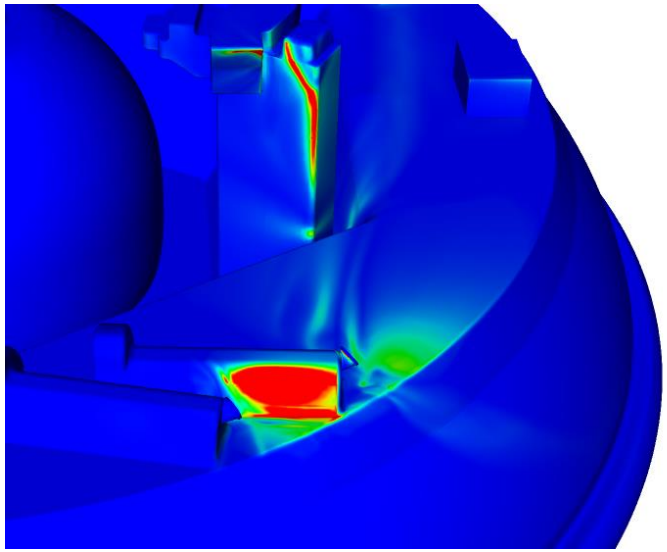

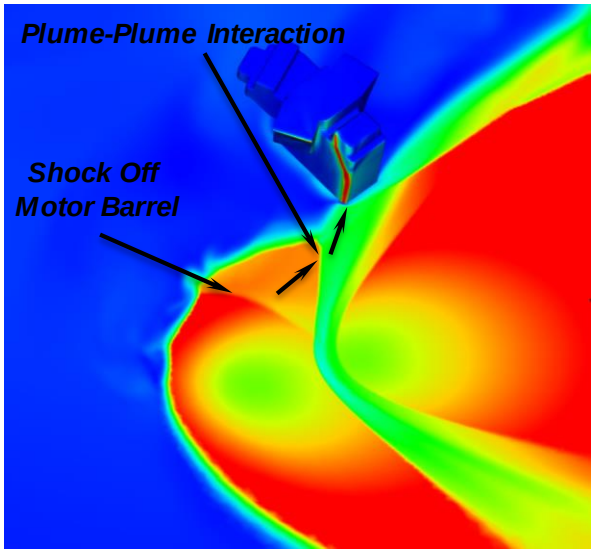

Surface Contours

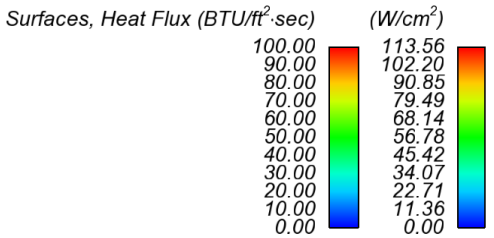

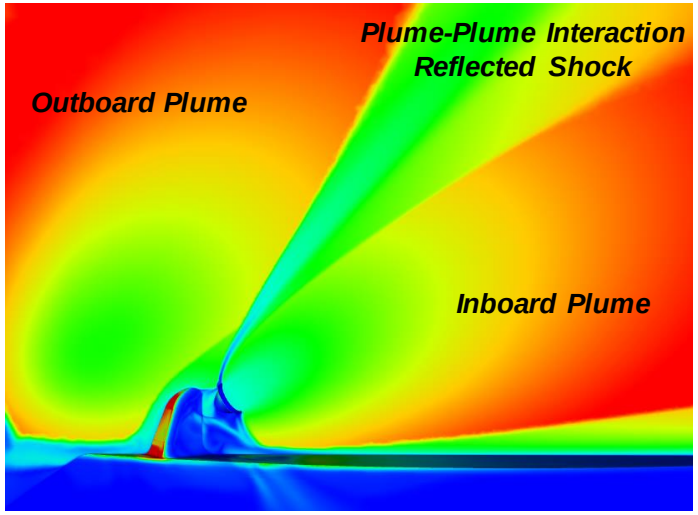

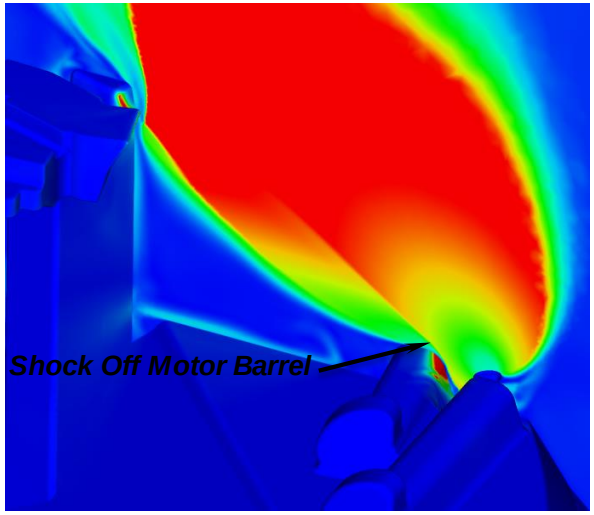

Solution Plane Contours

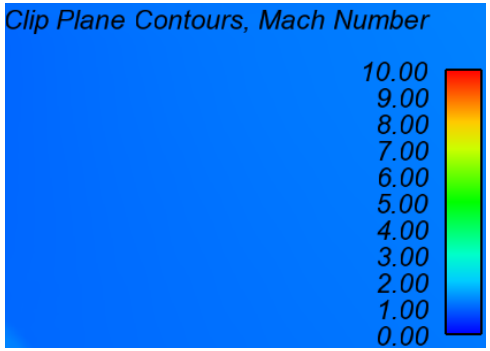

Spin Motor Analysis

- Initial Spin Motor Plume Impingement Summary
  - Motor casings, bridle coverings - severe heating areas, peak heat rates in excess of 500 BTU/ft^{2}sec (568 W/cm^2)
  - Camera mast, peak heat rates in excess of 200 BTU/ft^{2}sec (170 W/cm^2)

- Thermal and Operational Design Impacts
  - Two week “Tiger Team” to provide thermal protection options
  - Added plume deck blast shields, motor barrel shields and deflectors
    - Restricted height to prevent potential entanglement with chute brid. lines
  - Thermal protection (TPS) increased on camera mast (thin cork)
  - Staggered firing configurations (driven by flight dynamics, flight-ops as well)

Spin Motor Analysis

BEFORE INITIAL PLUME ANALYSIS

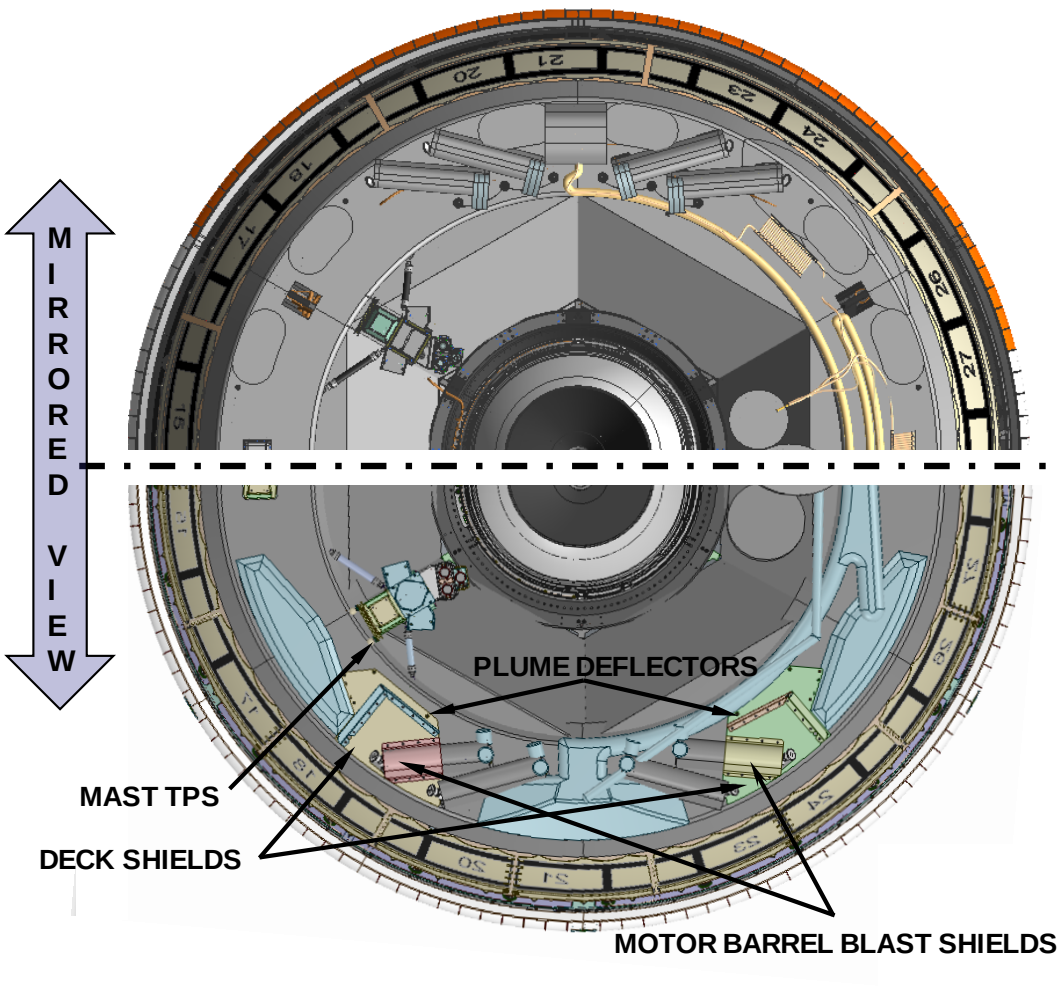

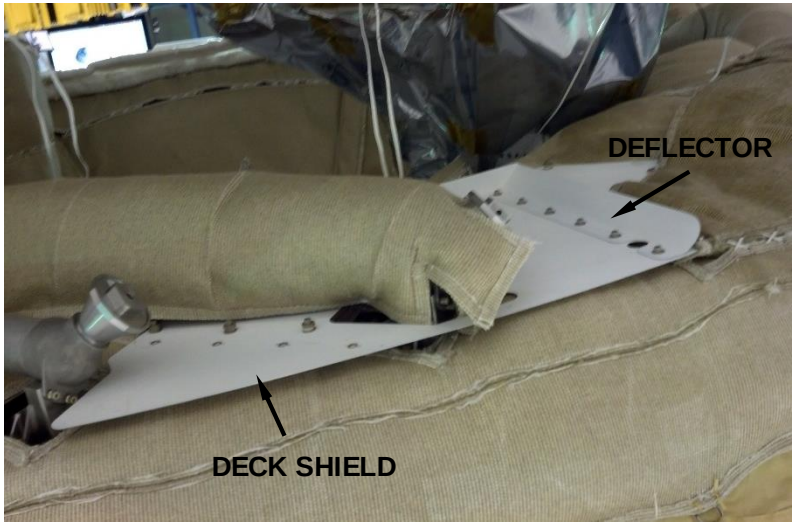

AFTER (MIRRORED PICTURE)

Spin Motor Analysis

FOLLOW-UP ANALYSIS

SPIN-UP – 120 Kft (36.6 km), P_∞= 0.72 PSIA (499 Pa) – STAGGERED FIRINGS

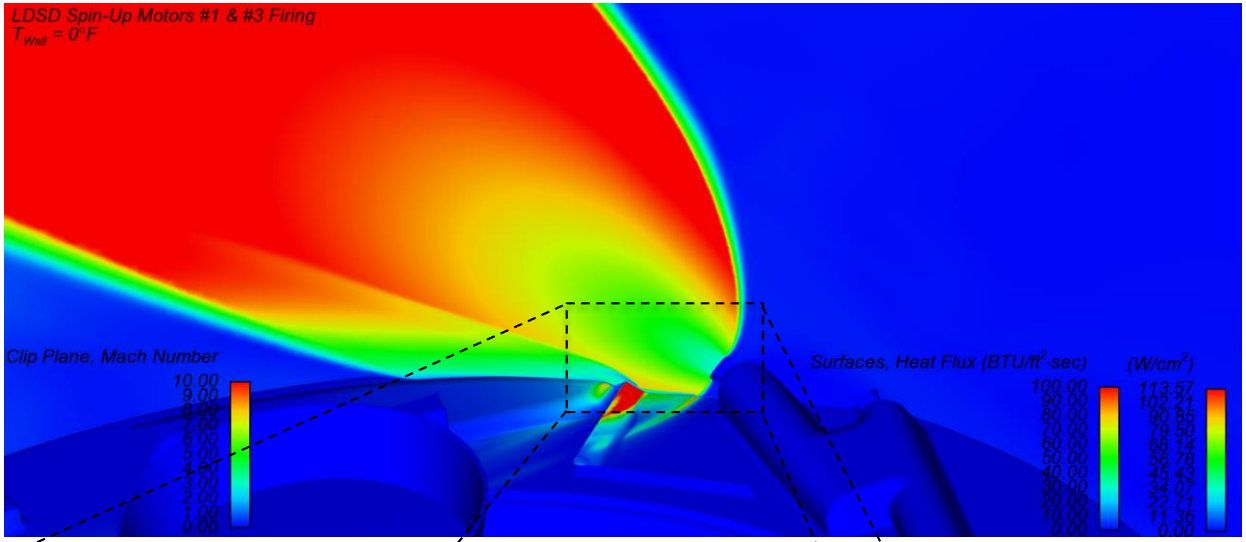

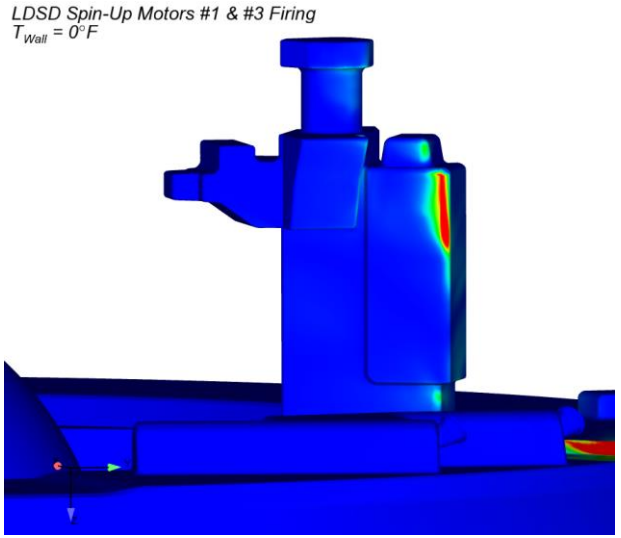

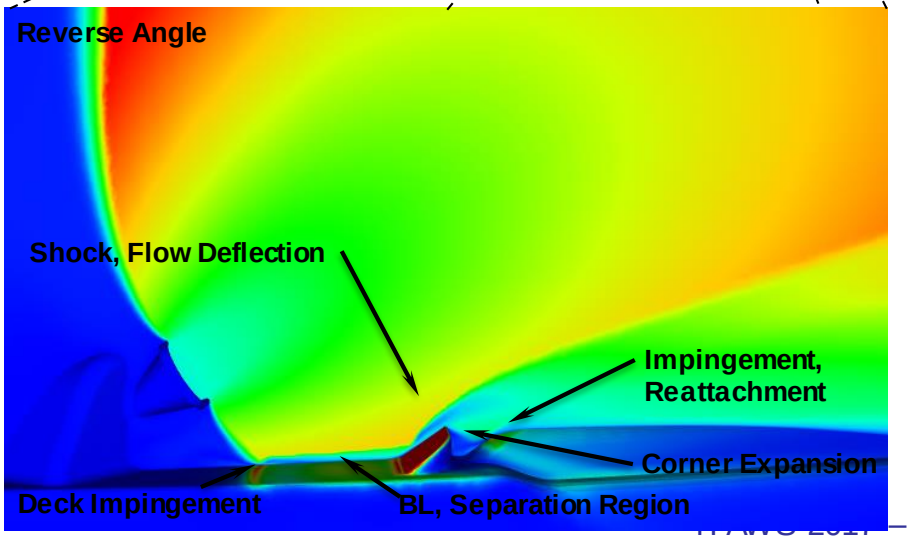

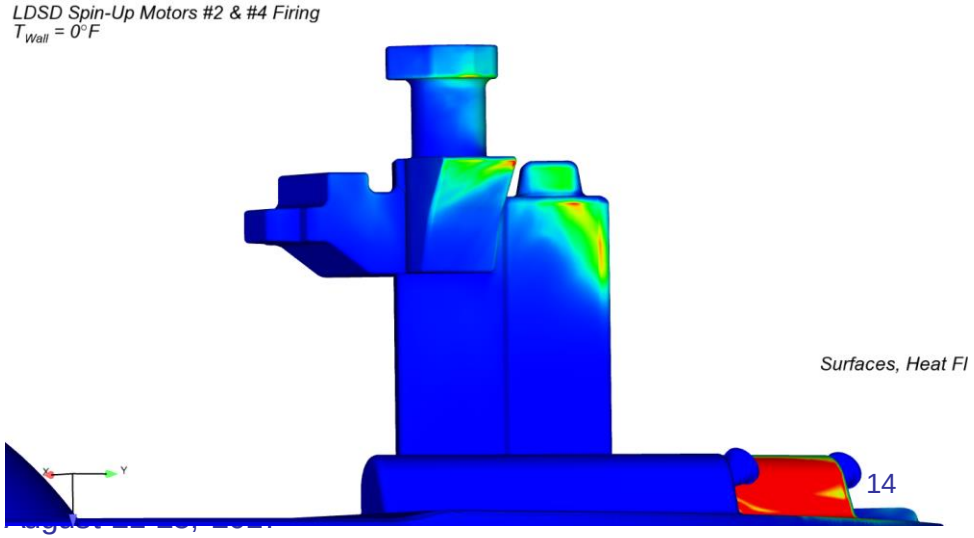

Spin Motor Results

SFDT-1 June 28, 2014

Spin-Up Motor Firings

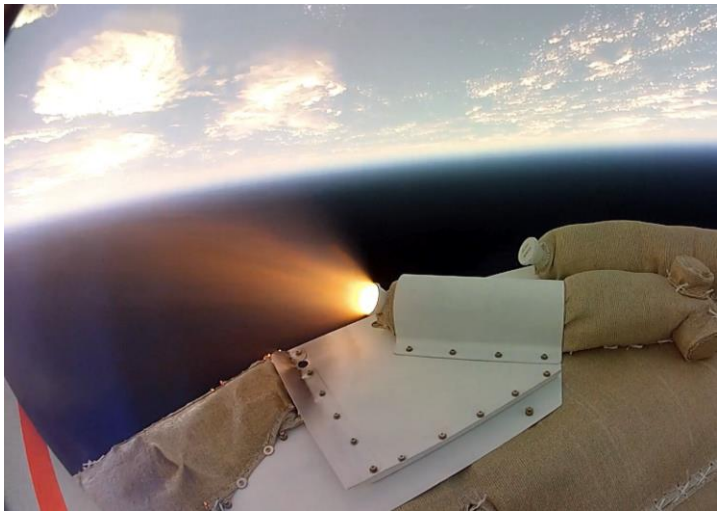

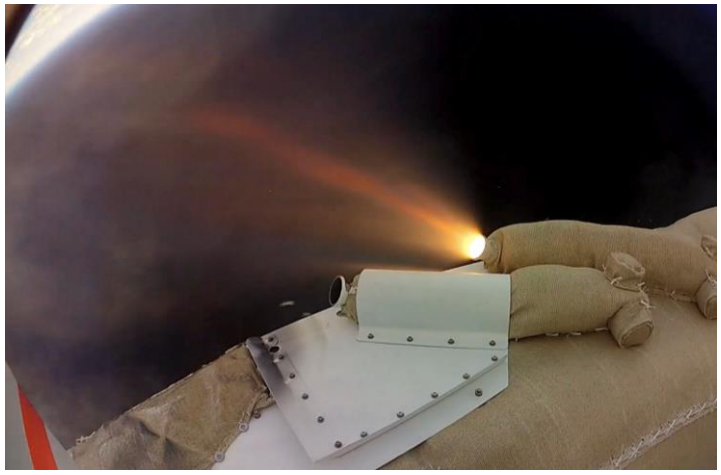

Pre-flight Heating Contours

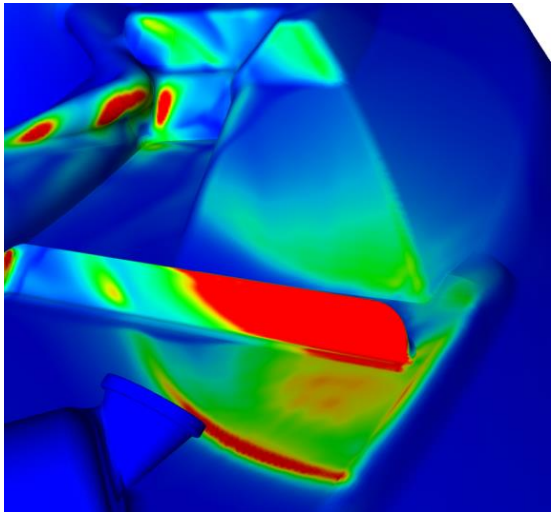

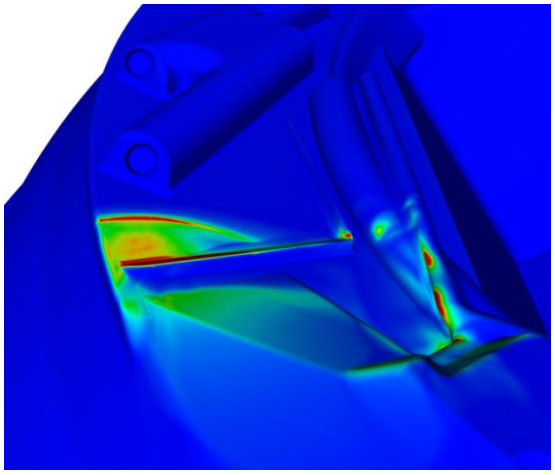

Post-flight Charring

Star 48 Analysis

- Pre-SFDT-1 Star 48 plume induced heating environments
  - Predicted radiation rates approximately a factor of 4 less than initial
  - Predicted base pressure coefficient always negative, predicted convective heat rates generally <1 BTU/ft^{2}sec
  - No thermal issues, **very benign**, highest temperatures were recorded on the Star 48 motor case (282 C, driven by internal environment)

Pre-SFDT-1 Convective Heating Prediction, 151Kft

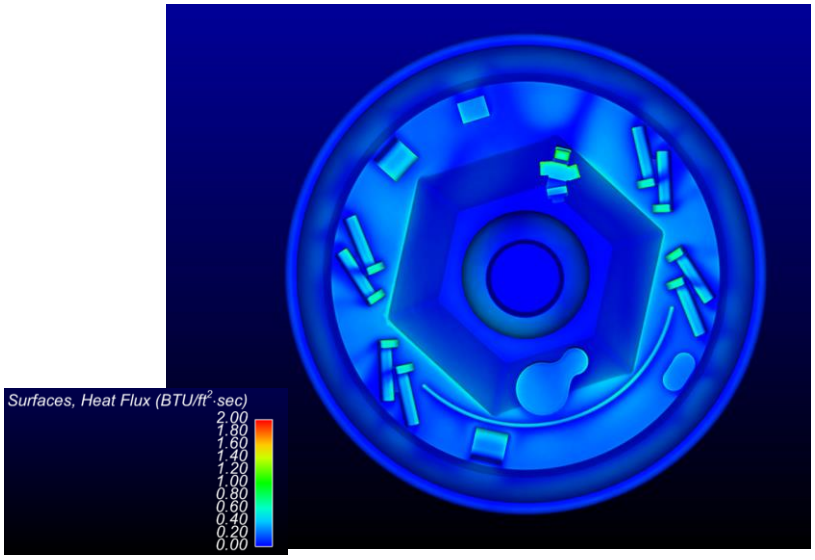

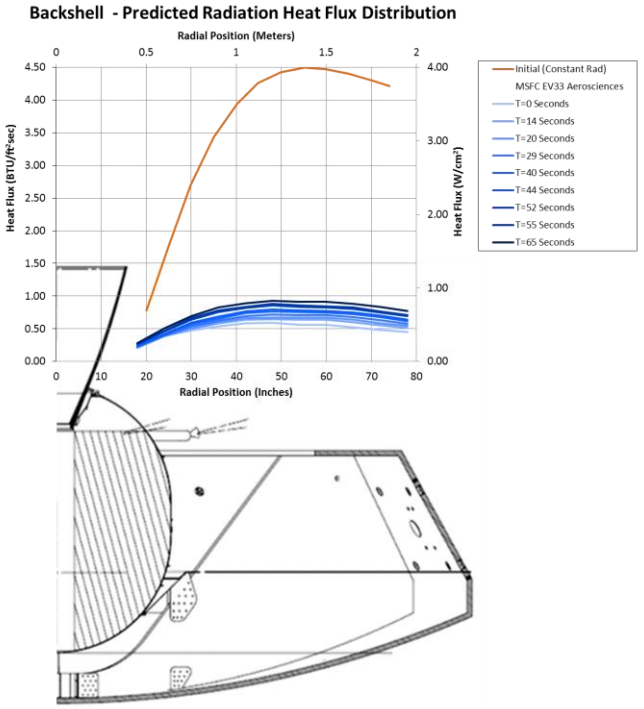

Star 48 Analysis

- SFDT-1 flight reconstruction revealed the test vehicle over shot the targeted altitude approximately 10Kft
  - No chamber pressure measurements, no distinct way to accurately decoupling thrust and drag (challenge on determination of C_A)
  - Thrust reconstruction analysis revealed slightly over performing solid and over prediction of plume induced drag
  - Over predicted total moment (pitch-yaw) coefficient, resulting in the vehicle lofting more than expected

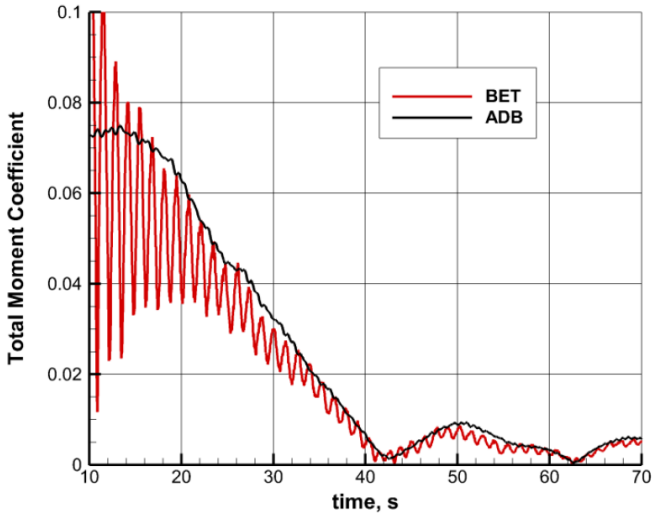

Figure Courtesy of John Van Norman, LaRC

Star 48 Analysis

- LDSD plume induced base flow field is different than "traditional" launch vehicles and missiles
  1. Blunt body - Realm of historical launch vehicles and missiles have a large slenderness ratio, where there is considerable running length to allow the development of a thick boundary layer that enters the base
  2. Ratio of base-to-nozzle exit area – free stream expansion angle entering the base, relative base eddy scale. Aft cavity provides recovery volume that affects the base environment
  3. Variation in total alpha due to spin/flight dynamics

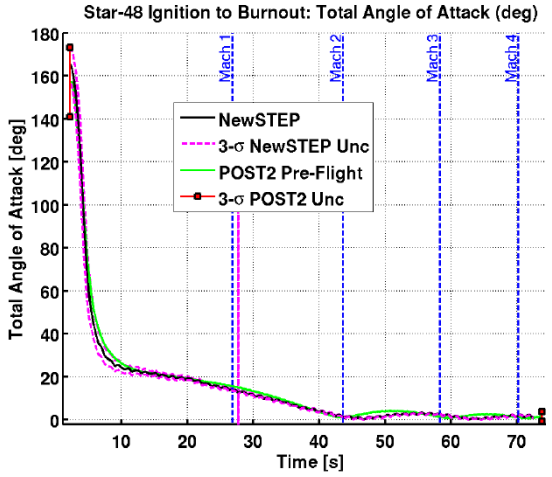

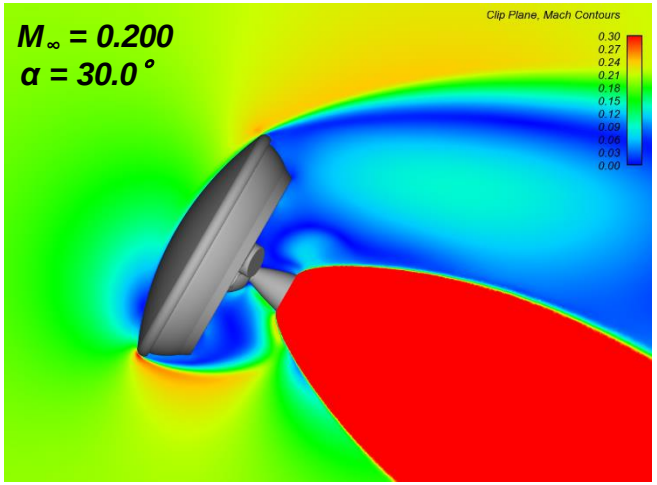

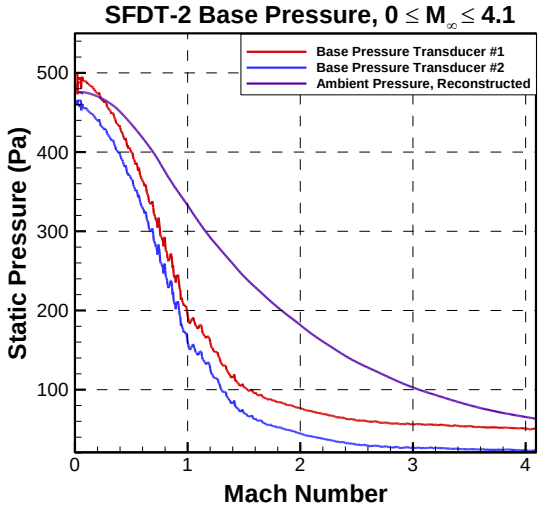

Figure Courtesy of Clara O'Farrell, JPL

Star 48 Analyses

Grid Evolution – Star 48

Initial Grids, Pre-SFDT-1 Heating (41 - 90 million cell, 2013)

- *Predominantly supersonic cases, 1.1 < M_∞ < 4.3, need higher q_∞ for recirculation*
- *Simple geometry & trajectory (α_{total}=0˚, small vol. O ~ 0.1 km^3)*
- *Primary objective, resolve forward shock, plume induced base recirc. (avg heating*

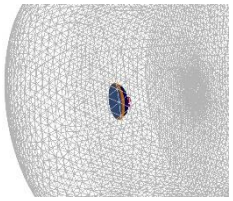

Post-SFDT-1 (90, 136 million, 2014)

- *Sub, transonic cases (M_∞= 0.5 - 1.2, "larger" vol. O ~ 1 km^3)*
- *Two geometries, reconstructed traj. subset (α, β = 0, 10, 20˚)*
- *Multiple Models – Plume w/wout particles, hybrid RANS/LES (423M)*
- *Objective, predict plume induced aero. forces & moments*

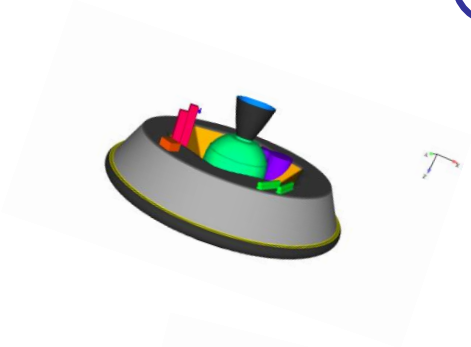

Pre-SFDT-2 (191 million, 2015)

- *Sub, transonic cases (M_∞=0 - 1.2 "larger" vol. O ~ 1 km^3)*
- *Reconstructed trajectory subset (α, β =10 – 40˚)*
- *Increase grid to accommodate ≥40˚ cases, seek grid convergence*

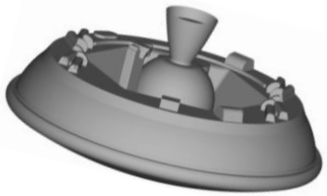

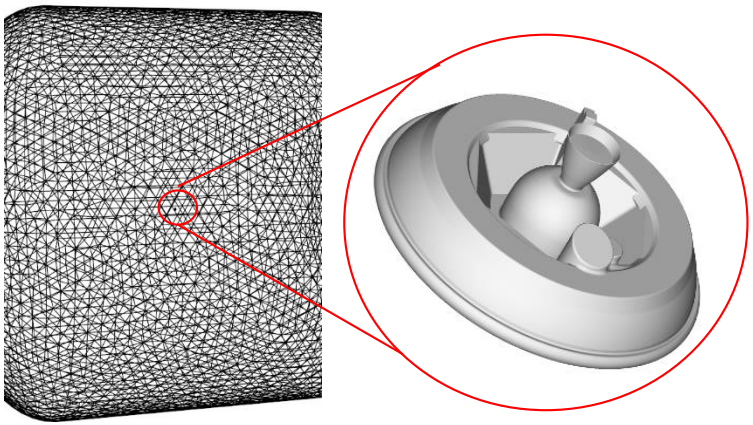

Type	Grid Cells (M)	Mach	α (deg)	CA	%ΔCA$_{ABS}$
Medium	136	0.5	20	1.1086	0.54%
Fine	192	0.5	20	1.1027	
Medium	136	0.9	20	1.2662	0.32%
Fine	192	0.9	20	1.2703	

Star 48 Analysis

Aerodynamic Database 1.5

OVERFLOW

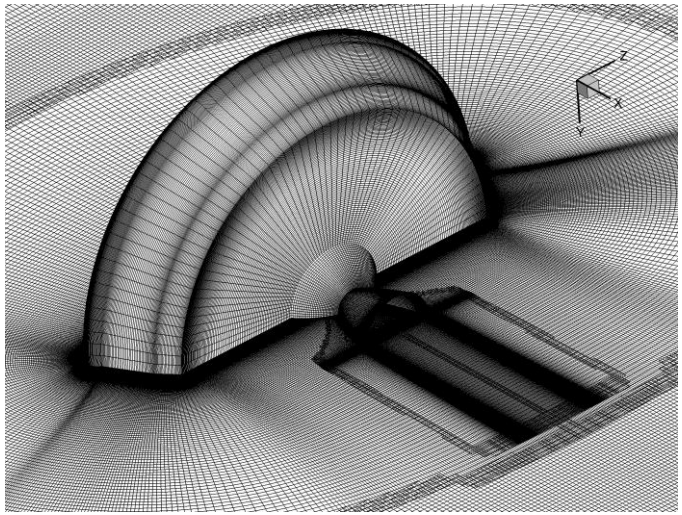

Loci-CHEM Runs (2015)

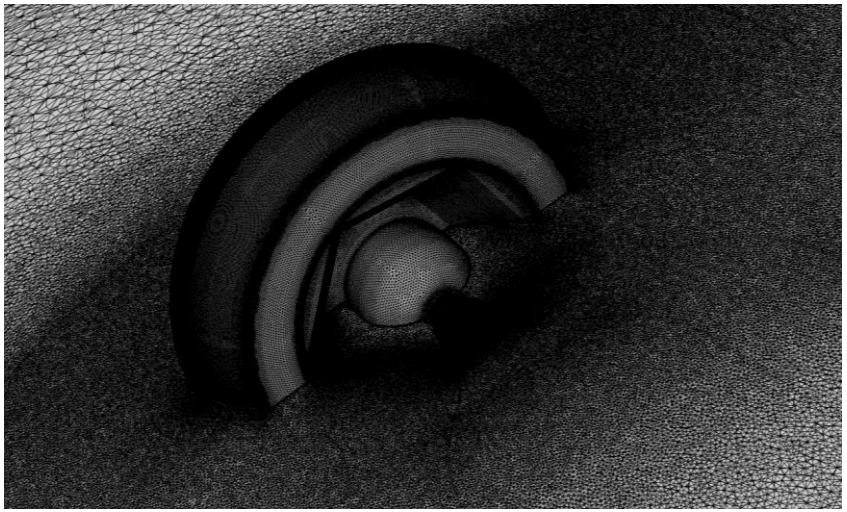

FUN3D

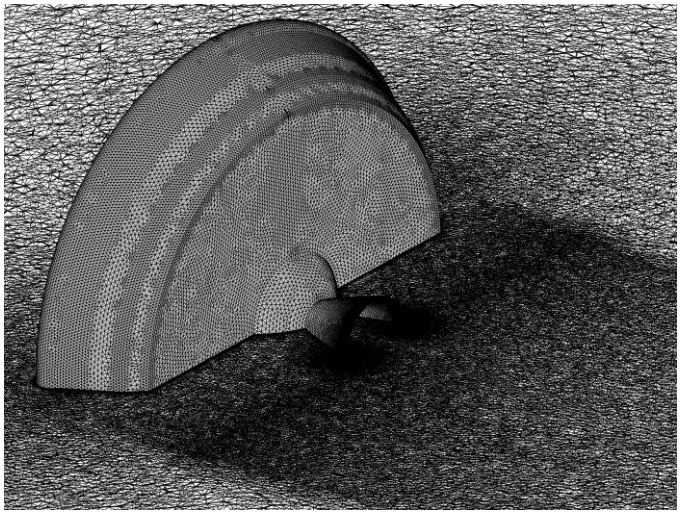

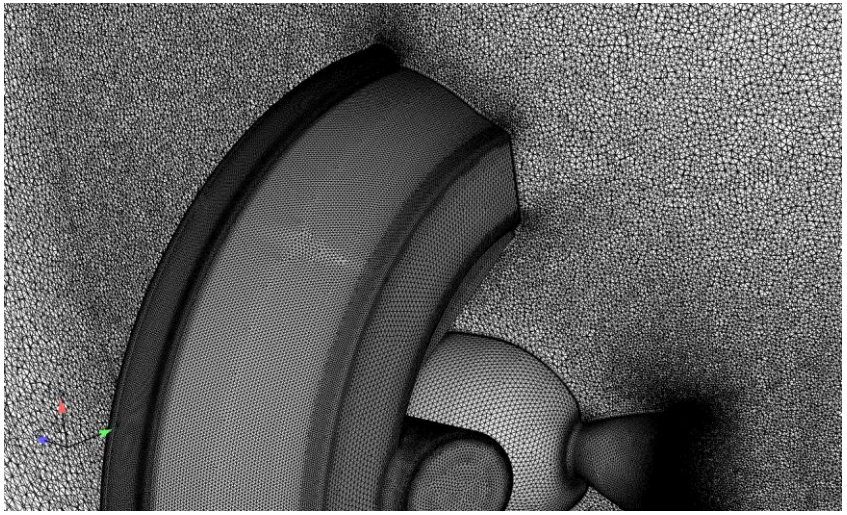

Figures[23] Courtesy of John Van Norman, LaRC

Star 48 Analysis

STAR48 PLUME INDUCED AERODYNAMICS

CFD, Mach = 0.7, Angle-of-Attack = 17.1˚

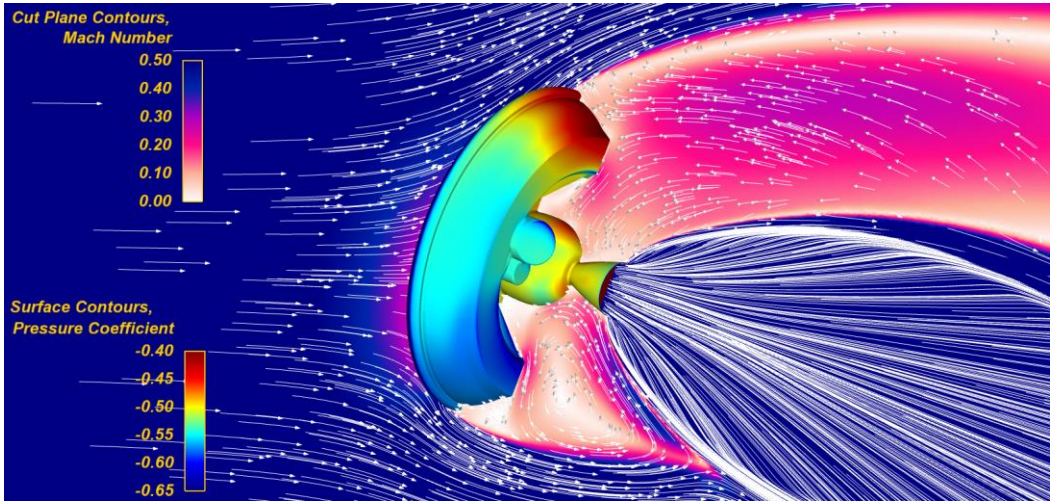

Base Pressure Coefficient

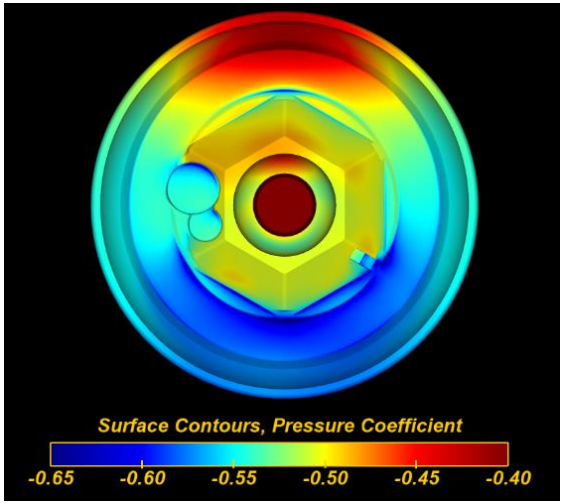

CFD, Mach = 1.2, Angle-of-Attack = 11.5˚

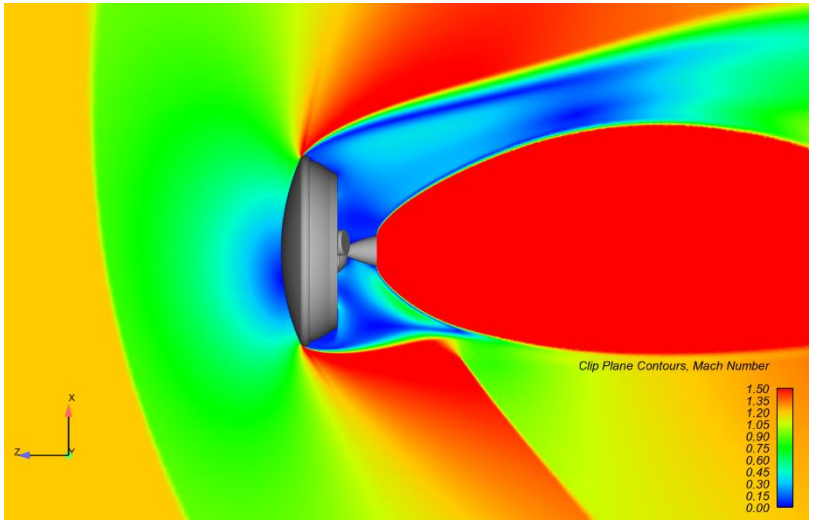

SFDT-1 Lofting Impact

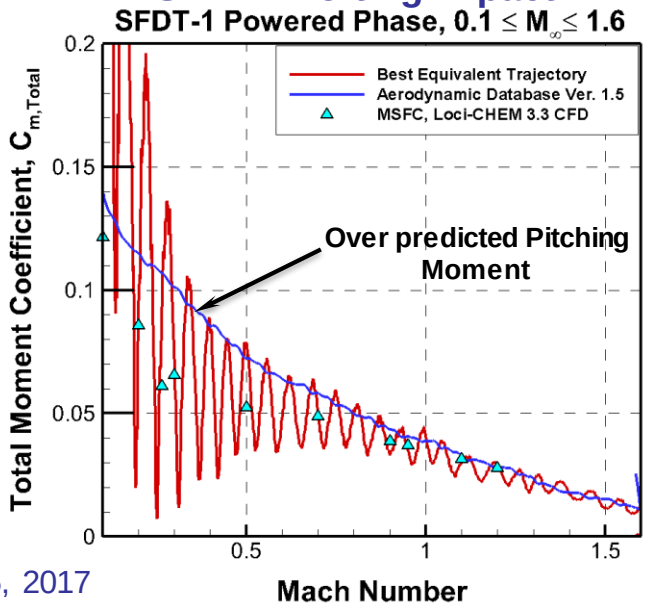

Star 48 Analysis

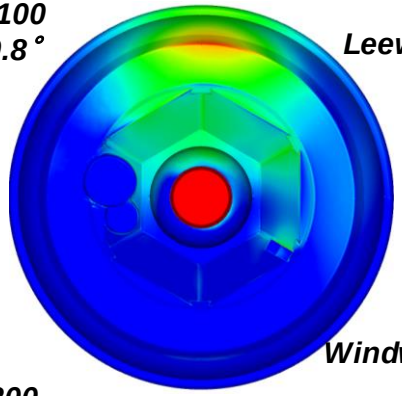

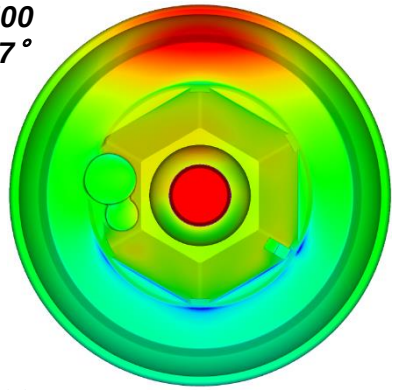

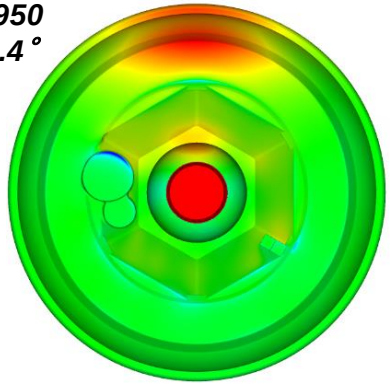

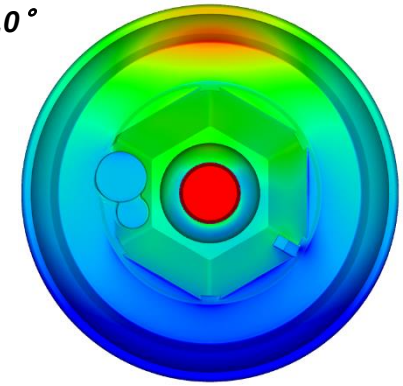

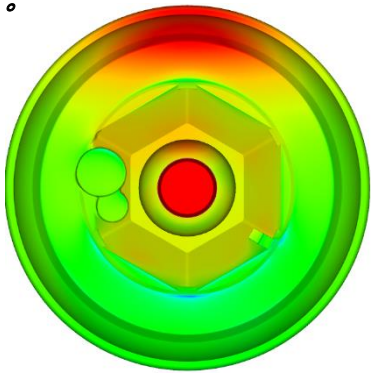

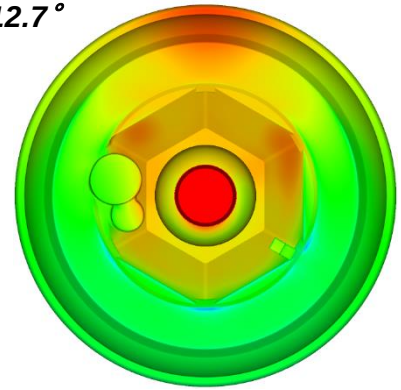

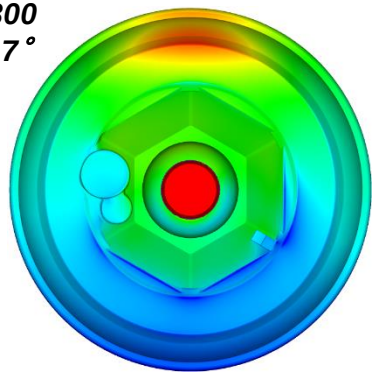

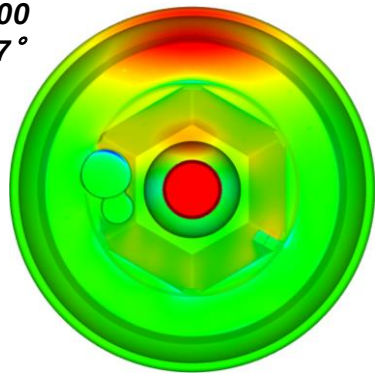

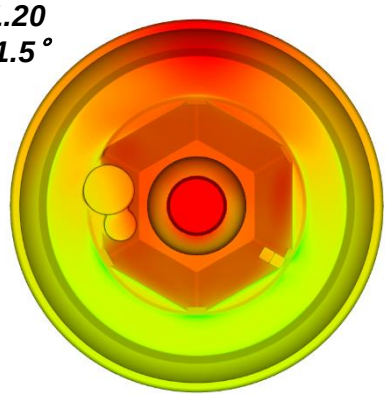

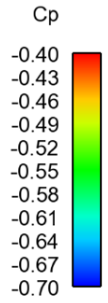

SFDT-2

- Flight Instrumentation
  - Star 48 chamber pressure, Kulite pressure transducer
    - Star 48 performance, thrust reconstruction
  - Tavis (2) pressure transducers (0-0.137 psia)
    - Base pressure, aero model CFD validation

Kulite pressure transducer

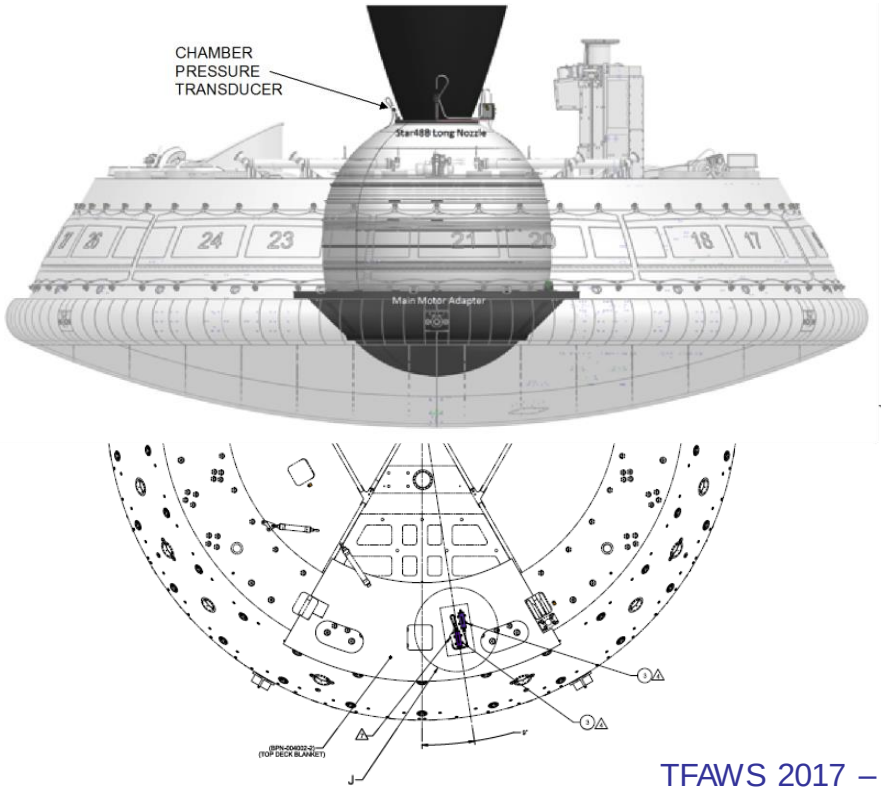

Tavis pressure transducers

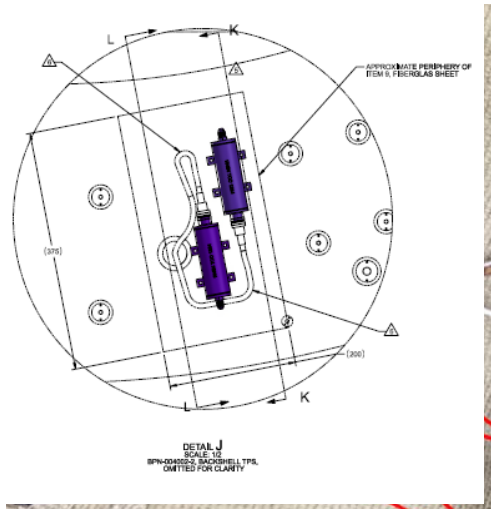

Impacts & Results

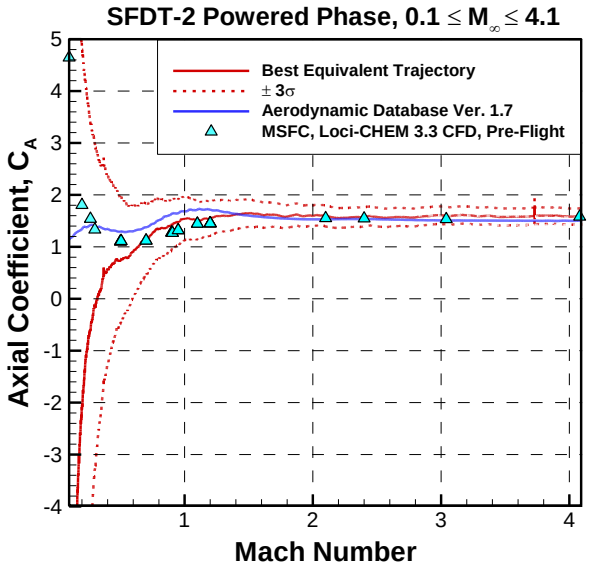

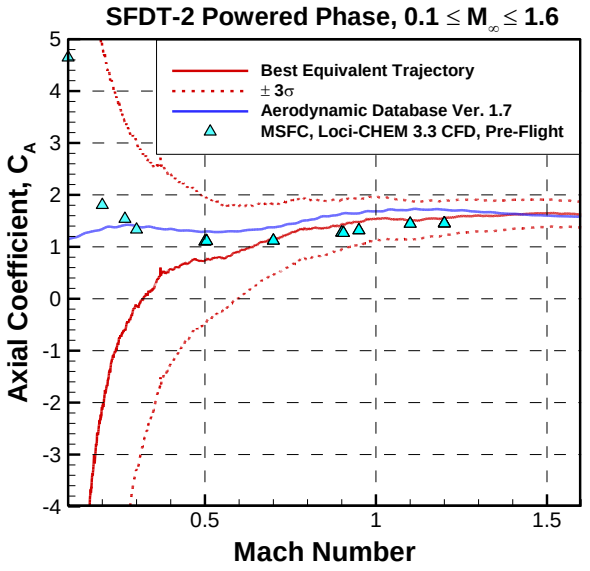

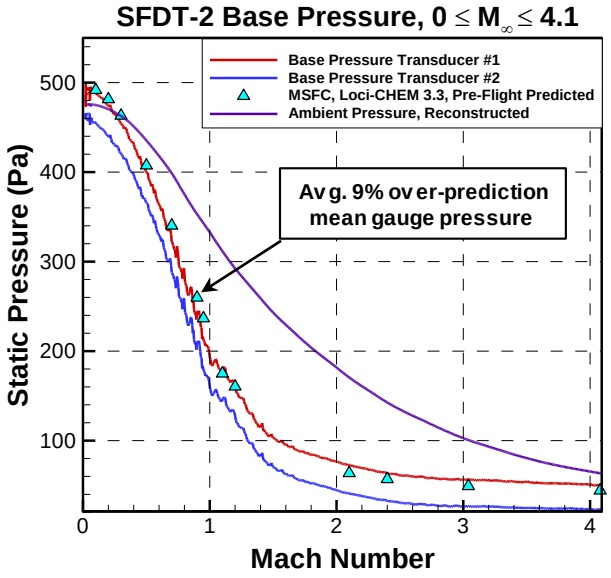

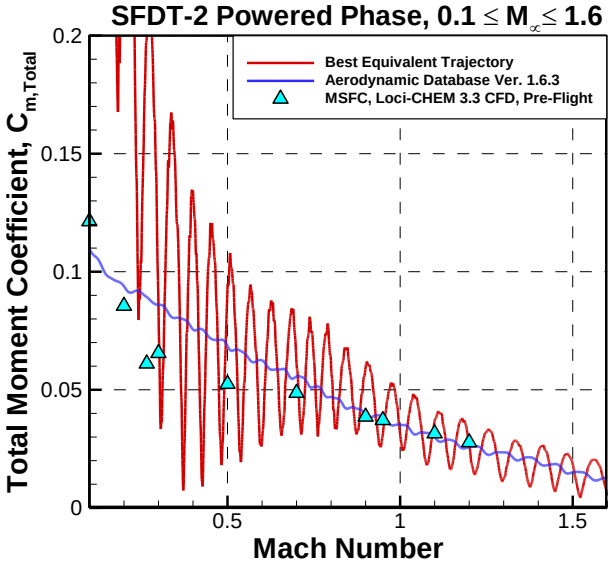

Conclusions & Lessons Learned

- Plume induced environments - all thermal requirements met[24], robust thermal design validated, Star 48 power-on aerodynamic data base updated (ready for potent. SFDT-3)
- Highly under expanded plume interactions can be significant
  - Degree of expansion, plume size, can lead to a variety of consequences!
  - Observed similar plume induced environment issues with sep. motors
  - Get plume modeling involved early in the analysis cycle
- Better understanding of the modelling sensitivities associated with single engine, plume induced base flow, in regards to the development of base eddy structure
  - Cavity geometry provided greater base pressure recovery, recirc. vortex interaction with base (similarly observed in base eddy studies)
  - Forward BL separation point, affects the point of impingement on Star 48 plume, momentum transfer interaction between base eddy and BL
  - Angle of attack, relative exposed plume area to the freestream
  - Match all nozzle exit conditions as best as possible

Questions

Questions?

Back-Up

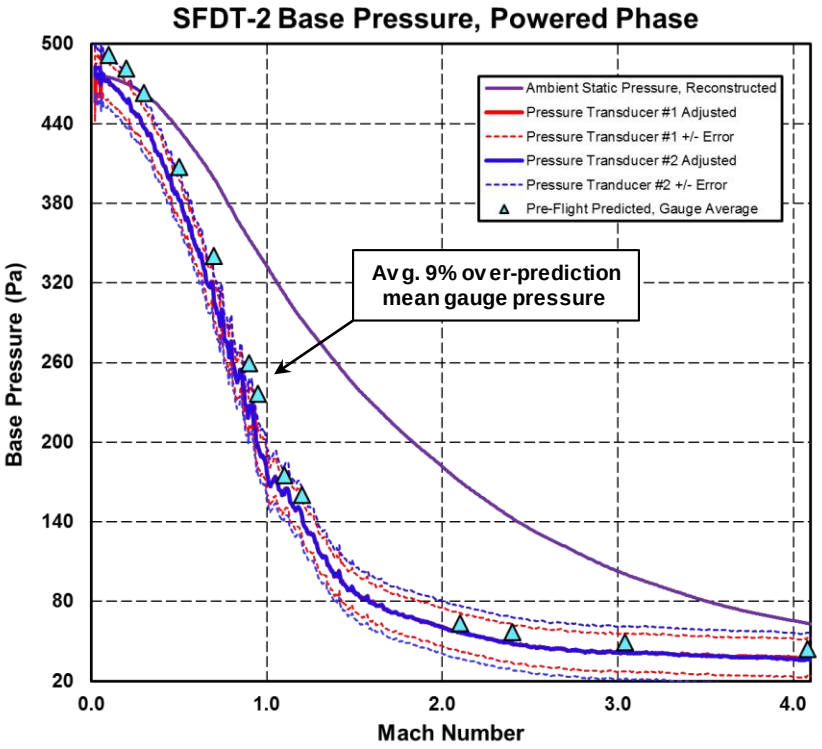
SFDT-2 Base Pressure, Powered Phase
Base Pressure (Pa)
Mach Number
Ambient Static Pressure, Reconstructed
Pressure Transducer #1 Adjusted
Pressure Transducer #1 +/- Error
Pressure Transducer #2 Adjusted
Pressure Tranducer #2 +/- Error
Pre-Flight Predicted, Gauge Average
Avg. 9% over-prediction mean gauge pressure

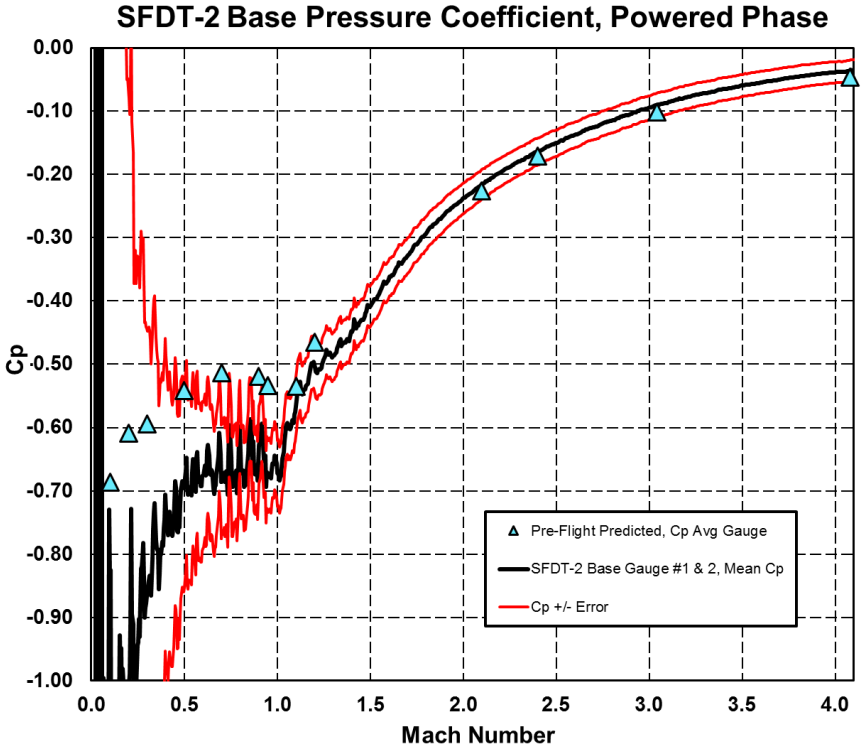
SFDT-2 Base Pressure Coefficient, Powered Phase
Cp
Mach Number
Pre-Flight Predicted, Cp Avg Gauge
SFDT-2 Base Gauge #1 & 2, Mean Cp
Cp +/- Error

Back-Up

Temperature Response[24]

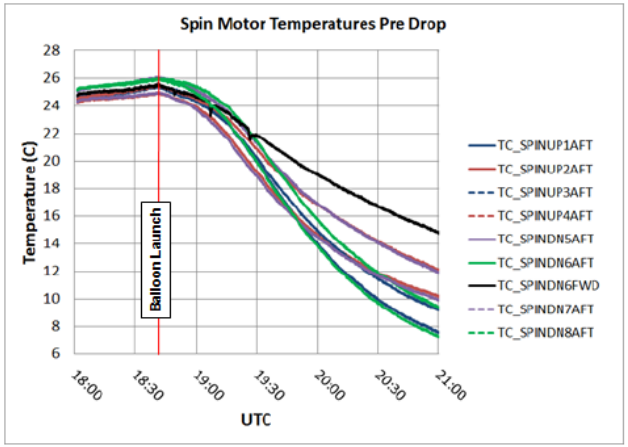

Figure 34. Spin Motor temperatures Pre Drop.

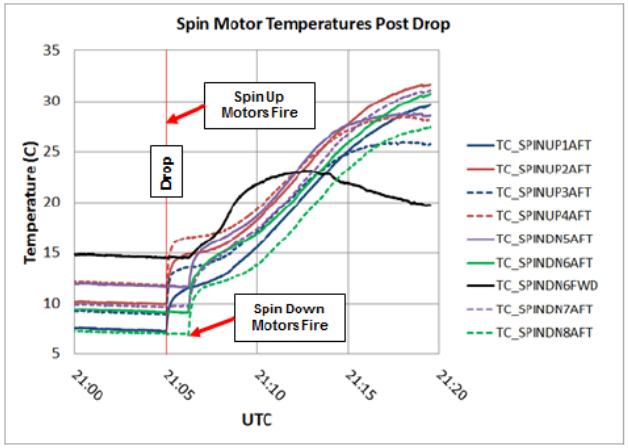

Figure 35. Spin Motor temperatures Post Drop.

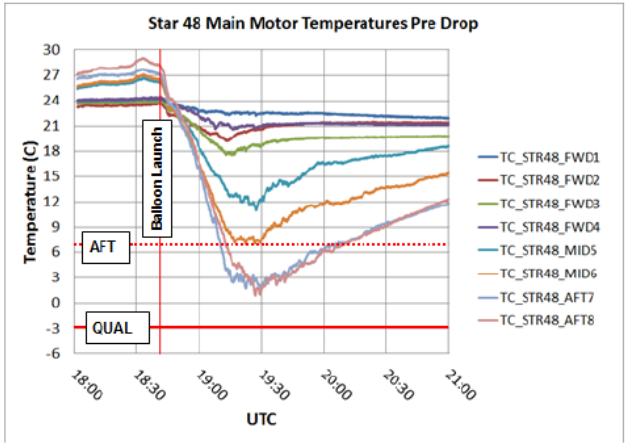

Figure 36. Star 48 Main Motor temperatures Pre Drop. AFT violation observed near nozzle during ascent.

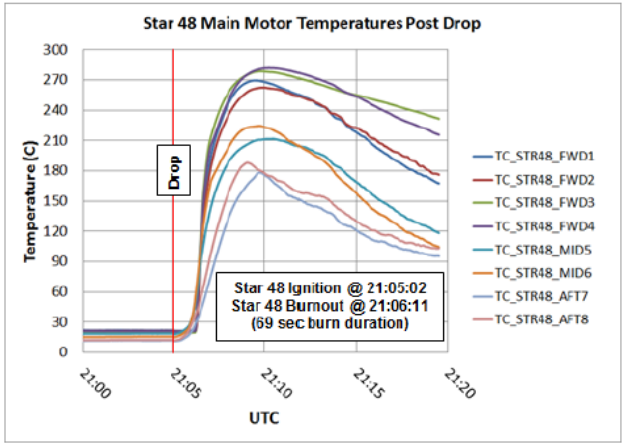

Figure 37. Star 48 Main Motor experienced soak back heating post engine burn up to a peak temp of 282°C.

Back-Up

Temperature Response[24]

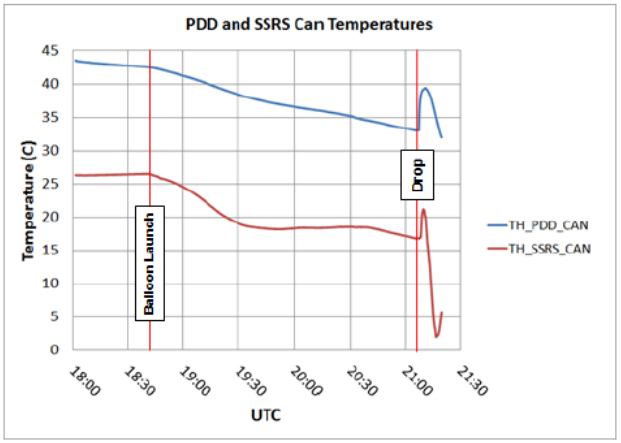

Figure 30. PDD and SSRS Canister temperatures. Inflation Aid within PDD canister likely at 44°C prior to deployment.

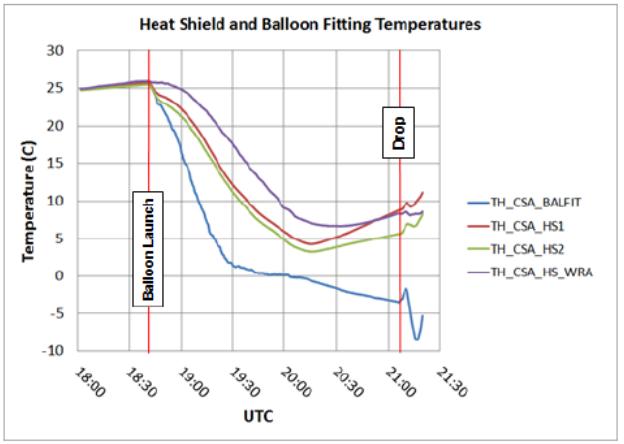

Figure 31. Heat Shield inner facesheet, Heat Shield Water Recovery Aid (WRA), and Balloon Fitting temperatures.

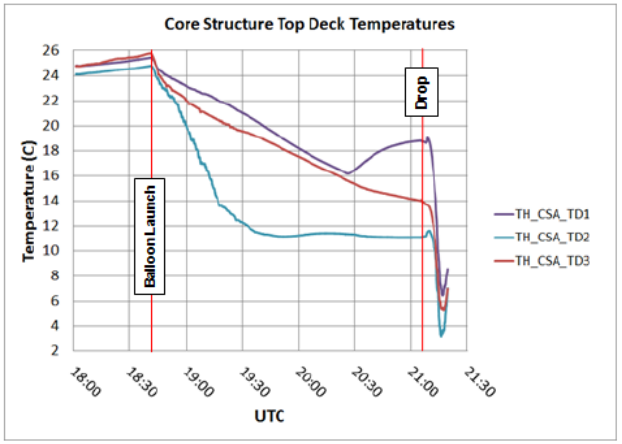

Figure 32. Core structure top deck outer facesheet temperatures.

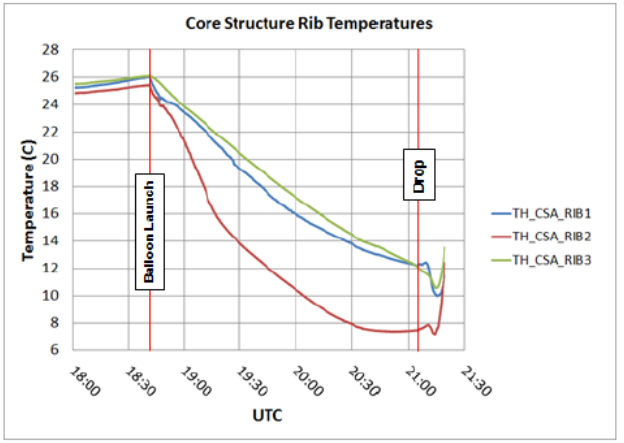

Figure 33. Core structure rib temperatures in vicinity of Star 48 Main Motor adaptor mounting ring.

Back-Up

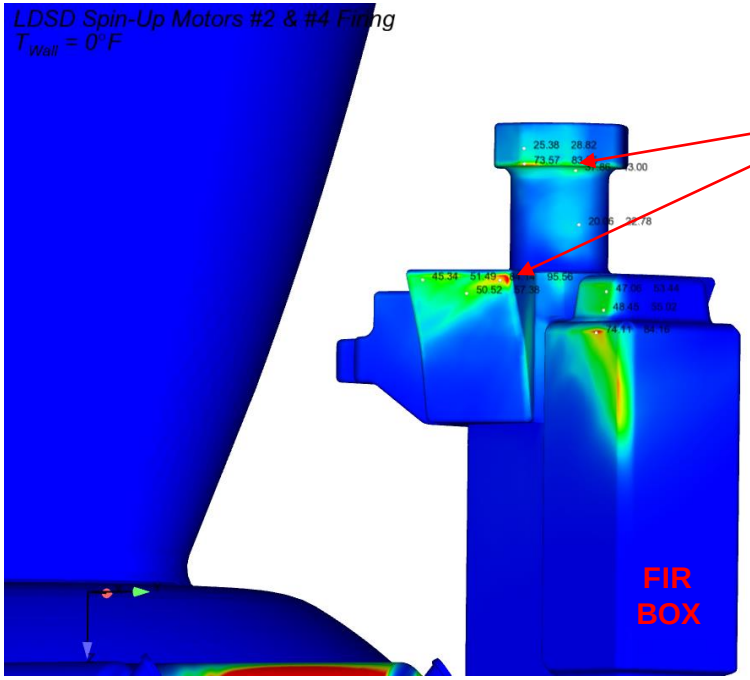

Surfaces, Heat Flux (BTU/ft^2·sec) (W/cm^2)

100.00	113.57
90.00	102.21
80.00	90.85
70.00	79.50
60.00	68.14
50.00	56.78
40.00	45.43
30.00	34.07
20.00	22.71
10.00	11.36
0.00	0.00

Back-Up

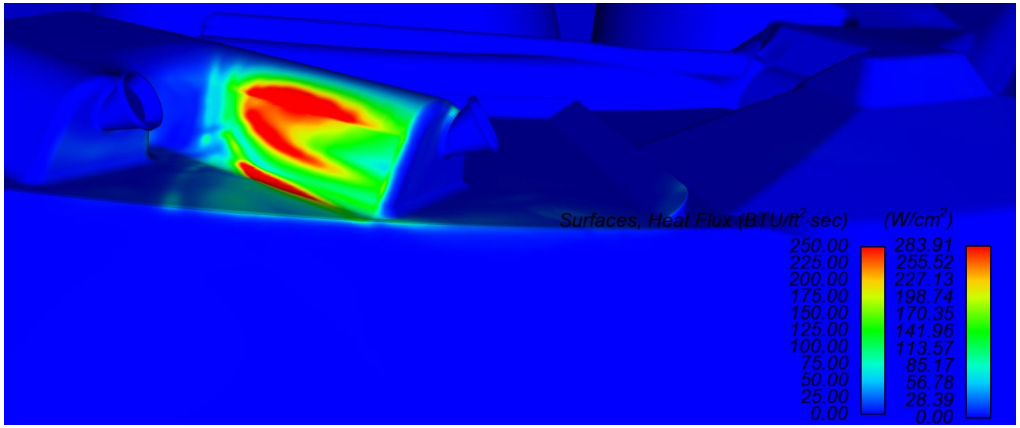
Surfaces, Heat Flux (BTU/ft²-sec) (W/cm²)
250.00 283.91
225.00 255.52
200.00 227.13
175.00 198.74
150.00 170.35
125.00 141.96
100.00 113.57
75.00 85.17
50.00 56.78
25.00 28.39
0.00 0.00

References

1. Muppidi, S., SFDT1_5p6_trajout_aero_ekf.mat, file received via email correspondence, Jul. 21, 2015.
2. Muppidi, S., SFDT1_6p3_trajout_aero_ekf.mat, file received via email correspondence, Aug. 25, 2015.
3. Orbital-ATK 2012 Motor Catalog, 2012 OA Motor Catalog.pdf, www.orbitalatk.com, October 2012.
4. Sulyma, P.R., and L.R. Baker, Jr., "User's Guide for TRAN72 Computer Code Modified for Use with RAMP and VOFMOC Flowfield Codes," LMSC HREC TM D390409, Lockheed Missiles & Space Company, Huntsville, Ala., October 1974.
5. Svehla, R.A., and B.J. McBride, "FORTRAN IV Computer Program for Calculation of Thermodynamics and Transport Properties of Complex Chemical Systems," NASA TN D 7056, January 1976.
6. Smith, S.D., "Update to the RAMP2 Computer Program", SECA FR 93 19, SECA Inc., Huntsville, AL., December 1993.
7. Evans, R.M., "Boundary Layer Integral Matrix Procedure BLIMPJ User's Manual," UN-75 64 Aerotherm, Mountain View CA., July 1975.
8. Bohern, C.F. and Huffman, D. R., Absorption and Scattering by Small Particles, John Wiley & Sons, Inc., 1983.
9. Luke, E., Tong, X-L., Wu, J., Tang, L., and Cinnella, P., "A Step Towards 'Shape Shifting' Algorithms: Reacting Flow Simulations Using Generalized Grids," 39th AIAA Aerospace Sciences Meeting and Exhibit, January 8–11, 2001, Reno, NV, AIAA Paper #2001-0897.
10. Liu, Q., Luke, E., and Cinnella, P., "Coupling Heat Transfer and Fluid Flow Solvers for Multi-Disciplinary Simulations," AIAA Journal of Thermophysics and Heat Transfer, Volume 19, No. 4, Oct.–Dec. 2005, pp417–427.
11. Wu, J., Tang, L., and Luke, E., "A Low Mach Number Preconditioning Scheme of the Reactive Roe Flux," 41st AIAA Aerospace Sciences Meeting and Exhibit, January 6–9, 2003, Reno, NV, AIAA #2003-0307.
12. Luke, E., "A Rule-Based Specification System for Computational Fluid Dynamics," Ph.D. Dissertation, Mississippi State University, December 1999.
13. Luke, E., and George, T., "Loci: A Rule-Based Framework for Parallel Multidisciplinary Simulation Synthesis," Journal of Functional Programming, Special Issue on Functional Approaches to High-Performance Parallel Programming, Vol.15, Issue 03, Cambridge University Press, 2005, pp477–502.
14. Luke, E., Tong, X., Wu, J., and Cinnella, P., "CHEM 3: A Finite-Rate Viscous Chemistry Solver – The User Guide", CHEM User Guide (Ver 3.3), Aug 2014.
15. Smith, S.D., "Development of a Nozzle/Plume and Plume Impingement Code," CI FR 0089, Continuum, Inc., Huntsville, AL, November 1986.
16. Taylor, M.W. and H.S. Pergament, "Standardized Plume Flowfield Model SPF3 Version 5 – Volume I, Model Formulation and Numerical Algorithms," PST-TR 60-I, Propulsion Science and Technology, Inc., Langhorne, PA, September 2005.
17. Smith, S.D., and J.E. Reardon, "Artificial Intelligence in Rocket Exhaust Plume and Plume Environments for Launch Vehicle and Spacecraft Design", HSC-FR-00-01, Huntsville Sciences Corp., Huntsville, AL, 10 January 2000.
18. Everson, J. and Nelson, H.F., "Development and Application of a Reverse Monte Carlo Radiative Transfer Code for Rocket Plume Base Heating," Journal of Thermophysics and Heat Transfer, 7 4, (1993)
19. Reardon, J. E. and Lee, Y. C., "A Computer Program for Thermal Radiation from Gaseous Rocket Exhaust Plumes," REMTECH RTR 014-9, December 1979.
20. Ludwig, C., et al, "Handbook of Infrared Radiation from Combustion Gases," NASA SP 3080 (1973).
21. Gaither, J., Marcum, D., and Mitchell, B., "SolidMesh: A Solid Modeling Approach to Unstructured Grid Generation," 7th International Conference on Numerical Grid Generation in Computational Field Simulations, September 2000
22. Marcum, D.L., "Advancing-Front/Local-Reconnection (AFLR) Unstructured Grid Generation," Computational Fluid Dynamics Review, World Scientific-Singapore, p. 140, 1998.
23. Van Norman, J., Presentation "SFDT_Aero_and_Power-On_Effects_032712.pptx" personal email correspondance, 2015.
24. Mastropietro, et. al., "First Test Flight Thermal Performance of the Low Density Supersonic Decelerator (LDSD) Supersonic Flight Dynamics Test (SFDT) Vehicle," ICES-2015-328, 45th International Conference on Environmental Systems, Bellevue, WA, 12-16 July 2015.